

Open-Loop Controller Design and Dynamic Characteristics of a Spherical Wheel Motor

Hungsun Son, *Member, IEEE*, and Kok-Meng Lee, *Fellow, IEEE*

Abstract—This paper presents a control system design for a particular form of variable-reluctance spherical motors, referred to here as a spherical wheel motor (SWM). The method decoupling the spin from the inclination offers a means to control, in open loop (OL), the inclination of a continuously rotating shaft. Specifically, the OL controller presented in this paper combines a multispeed switching control law for controlling the spin motion and a dynamic model-based control law for regulating the rotor inclination of an SWM. The concept feasibility of the OL-controlled SWM (consisting of permanent magnets in a rotor and electromagnets in a stator) has been experimentally demonstrated. The experimental study not only demonstrates the design procedure but also provides intuitive insights into the effects of key operation parameters on the SWM dynamics. The results presented here will serve as a basis for developing feedback controllers for increasing accuracy and robustness for disturbance rejection.

Index Terms—Electromagnets (EMs), magnetic dipole, magnetic field, multi-degree-of-freedom (DOF) actuator, open-loop (OL) control, stepping motor.

I. INTRODUCTION

MANY MOBILE vehicles such as wheels [1], propellers [2] for boats, helicopters or underwater vehicles, robotic joints, and machine tools require orientation control of the rotating shaft. Existing designs are typically combined with single-axis devices; thus, orientation control of their rotating shafts must be manipulated by an external mechanism. These multi-axis spinners are generally bulky, slow in dynamic response, and have a lack of dexterity in negotiating the orientation of the rotating shaft. This paper presents a spherical wheel motor (SWM), an alternative design built upon the concept of a variable reluctance spherical motor (VRSM) originally conceptualized in [3]. The SWM, much like the VRSM that is capable of offering 3 degrees of freedom (DOF) in a single joint, is essentially a ball-joint-like brushless direct-drive actuator. However, unlike the VRSM which has been mainly designed to

control its 3-DOF angular displacements, the SWM discussed here offers a means to control the orientation of the rotating shaft in the single spherical joint. Several different multi-DOF motor designs such as direct current motors [4] and piezoelectric actuators [5] have been proposed. We focus here on the development of a permanent-magnet (PM)-based 3-DOF spherical motor which has gained increasing attention during the last decade because of its simplicity in structure and compact in design. Several design variations [6], [7] with a structure similar to that in [3] have been studied. There are also studies on design configurations [8], magnetic field and torque models [9]–[13], 3-DOF orientation control [13]–[15], and practical applications [14], [15]. These existing spherical motors (motivated by the advance in robotic technology) have predominantly been designed for wristlike motions. While previous studies primarily focused on controlling the 3-DOF rotational displacements in closed loop, this paper investigates the feasibility of developing a spherical motor that achieves the dexterous orientation control of a rotating shaft in open loop (OL).

Electromagnetic actuators utilizing PMs have been controlled by both OL and closed loop. However, closed-loop control systems for a nonlinear electromagnetic actuator have difficulties due to a number of uncertainties involving system identification and force/torque computation [16]. In particular, it is much more difficult to design multi-DOF spherical motors as well as develop their control system due to their nonlinear rotor dynamics, intricate magnetic fields, and challenging measurement problems. Nevertheless, controller design techniques for a single-axis actuator can be extended to a multi-DOF spherical motor particularly when it has the capability to operate in OL.

A number of electromagnetic actuators have been demonstrated using an OL controller. In [17], an OL controller manipulated a stepping motor with respect to the torque equilibrium position. The controller successfully performed to suppress rotor oscillation and is also insensitive to the variation of motor dynamics, which is crucial for the motor control since the motor has a large unknown payload. In [18], an instantaneous torque control scheme with improved torque estimation and control characteristics has been proposed to a direct-drive PM synchronous motor. Recently, the interest to develop an OL stable spherical motor has led to the concept of an SWM operated on a push-pull principle in [7] and a distributed multipole (DMP) method to analyze the magnetic field of a PM in a closed-form solution [19]. Illustrations of the DMP method for deriving the torque model of a spherical motor can be found in [20] and [21]. In this paper, the DMP method has been extended to the design of a model-based controller for operating the SWM in OL.

Manuscript received December 14, 2008; revised July 2, 2009, September 17, 2009, September 21, 2009; accepted November 30, 2009. Date of publication February 5, 2010; date of current version September 10, 2010. This work was supported in part by an SUG Grant from Nanyang Technological University, by a Tier 1 Grant from MOE, Singapore, by the U.S. Poultry and Eggs Association, and by the Georgia Agricultural Technology Research Program.

H. Son is with the School of Mechanical and Aerospace Engineering, Nanyang Technological University, Singapore 639798 (e-mail: hsson@ntu.edu.sg).

K.-M. Lee is with the George W. Woodruff School of Mechanical Engineering, Georgia Institute of Technology, Atlanta, GA 30332-0405 USA (e-mail: kokmeng.lee@me.gatech.edu).

Color versions of one or more of the figures in this paper are available online at <http://ieeexplore.ieee.org>.

Digital Object Identifier 10.1109/TIE.2009.2039454

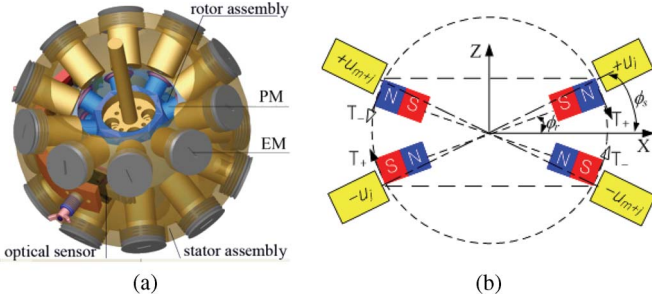


Fig. 1. Schematics illustrating the mechanical structure of an SWM. (a) CAD model [7]. (b) Stator and rotor pole pairs.

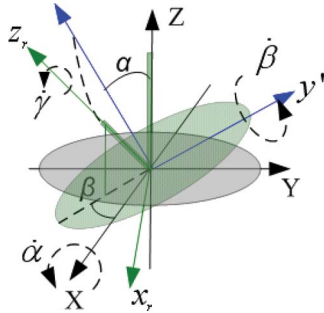


Fig. 2. XYZ coordinate transformation.

The remainder of this paper offers the following.

- 1) This paper presents the electromechanical structure and the dynamic model of an SWM designed for manipulating the inclination of a continuously rotating shaft. As will be shown, the magnetic torque model in a closed form plays an essential role in the design of the OL-controlled SWM and the prediction of its dynamics.
- 2) An OL controller for the SWM has been developed. The controller consists of two parts, decoupling the spin motion from the inclination control: a multispeed-level switching law for regulating the spin rate and the inverse torque model for manipulating the inclination.
- 3) Numerical simulations and experiments have been shown to illustrate the effectiveness of the OL controller on a prototype SWM consisting of 20 stator electromagnets (EMs) and 16 rotor PMs. The experimental results verify the control system design and offer intuitive insights into the effects of key design parameters on the SWM dynamics.

II. MECHANICAL STRUCTURE AND DYNAMIC MODEL

Fig. 1 shows the CAD model of the SWM consisting of 16 rotor PMs and 20 stator EMs equally spaced on four circular planes. As shown in Fig. 1(b), the PMs and EMs are grouped in pairs, and every two pairs form a plane, and their magnetization axes pass radially through the center with opposite polarities (S and N indicate the south and north polarities, respectively). The rotor and stator of the SWM are spherically symmetric with respect to both electrical and mechanical configurations. The magnetization axes of the m_r rotor PM pairs and m_s stator EM pairs are given by (1) and (2) in their own body coordinate frames shown in Figs. 1 and 2, respectively,

$$\mathbf{r}_k = (-1)^{k-1} [\cos \phi_r \cos \delta_{rk} \quad \cos \phi_r \sin \delta_{rk} \quad \sin \phi_r]^T \quad (1)$$

where the subscript rk indicates the k th PM pair of the rotor. $\delta_{rk} = (k-1)\delta_r$, where $k = 1, 2, \dots, m_r$ and $\delta_r = 2\pi/m_r$

$$\mathbf{s}_j = [\cos \phi_s \cos \delta_{sj} \quad \cos \phi_s \sin \delta_{sj} \quad \sin \phi_s]^T \quad (2)$$

where the subscript sj denotes the j th EM pair of the stator. $\delta_{sj} = (j-1)\delta_s$, where $j = 1, 2, \dots, m_s$ and $\delta_s = 2\pi/m_s$.

In (1) and (2), ϕ_r and ϕ_s are the angles between the magnetization axes and the XY plane defined in Fig. 1(b). Unlike m_s , which may be odd or even in general, m_r is always an even number to maintain the symmetry. The SWM is operated on a push-pull principle with two opposing torques (\mathbf{T}_+ and \mathbf{T}_-) maintaining its rotor at zero inclination about an axis that is normal to the plane containing the current inputs, $\pm u_j$ and $\mp u_{m+j}$ as shown in Fig. 1(b). The specific polarities of the EMs depend on the PM layout; for example, $|u_j| = |u_{m+j}|$ with different polarities in Fig. 1(b).

A. Torque Model

Magnetic forces involved in the SWM can be calculated using the Lorentz force equation

$$\mathbf{F} = - \int \mathbf{B} \times \mathbf{I} d\ell, \quad \mathbf{I} = \int \int \mathbf{J} \bullet d\mathbf{S} \quad (3)$$

where \mathbf{B} is the magnetic field generated by PMs, \mathbf{I} is the current input through the conductor, and ℓ is a normalized vector of the current direction. In (3), since the current density vector \mathbf{J} is used in the calculation, it is not necessary to compute the magnetic field generated by the current loop. Thus, the Lorentz force calculation involves only the \mathbf{B} fields of the PMs. The magnetic field \mathbf{B} of the PMs can be computed by the DMP method [19], which provides the solution in a closed form. However, the PMs rotate with respect to the stator EMs. To compute the force acting on the current-carrying j th EM, the total magnetic field \mathbf{B} is expressed in the j th EM coordinates \mathbf{r}_{cj} .

Fig. 2 shows the $X'y'z_r$ Euler angles (α, β, γ) which have no singularity in the domain of interest ($-20^\circ \leq \alpha, \beta \leq 20^\circ$, and $-\infty \leq \gamma \leq \infty$) for the coordinate transformation from the rotor to the stator. In the local coordinate system of the j th EM, the position of the k th PM is given by

$$\mathbf{r}_{cj} = [\mathbf{L}_{js}] [\mathbf{L}_{sr}] \mathbf{r}_k \quad (4)$$

where

$$[\mathbf{L}_{sr}] = \begin{pmatrix} C_\gamma C_\beta & C_\gamma S_\alpha S_\beta & -C_\gamma C_\alpha S_\beta + S_\gamma S_\alpha \\ -S_\gamma C_\beta & C_\alpha C_\gamma - S_\gamma S_\alpha S_\beta & S_\gamma C_\alpha S_\beta + C_\gamma S_\alpha \\ S_\beta & -S_\alpha C_\beta & C_\alpha C_\beta \end{pmatrix}$$

$$[\mathbf{L}_{js}] = \begin{pmatrix} C_{\phi_s} & -S_{\phi_s} & 0 \\ S_{\delta_{sj}} S_{\phi_s} & S_{\delta_{sj}} C_{\phi_s} & C_{\delta_{cj}} \\ -C_{\delta_{sj}} S_{\phi_s} & -C_{\delta_{sj}} C_{\phi_s} & S_{\delta_{cj}} \end{pmatrix}$$

with C and S representing the cosine and sine of the subscript denoting the angle, respectively.

Once the force acting on the j th EM is computed, the resultant torque for all EMs can be computed from (5) using the Lorentz formulation [20]

$$\mathbf{T}_{\text{total}} = [T_X \quad T_Y \quad T_Z]^T = [\tilde{\mathbf{T}}_1 \quad \tilde{\mathbf{T}}_2 \quad \dots \quad \tilde{\mathbf{T}}_{m_s}] \mathbf{u} \quad (5)$$

where

$$\tilde{\mathbf{T}}_j = \mathbf{L}_{j_s}^T \left(\iiint_{EM} \left[\sum_i m_i \beta_i(\alpha, \beta, \gamma) \right] dS dl \right) \in \mathbb{R}^{3 \times 1} \quad (5a)$$

$$\mathbf{u} = [J_1 \quad J_2 \quad \cdots \quad J_{m_s}]^T \quad (5b)$$

with m_i and $\beta_i(\alpha, \beta, \gamma)$ being the dipole moment and element of the DMP model, respectively.

The orientation-dependent torque vector (5) must be volume integrated numerically in real time. To reduce the computation to a tractable form, the torque is expressed as a linear function of current vector \mathbf{u} . By using the principle of superposition in [9], the total magnetic torque acting on the rotor can be computed from the following equation in stator coordinates:

$$\mathbf{T}_{\text{total}} \approx [\hat{\mathbf{K}}_1 \quad \cdots \quad \hat{\mathbf{K}}_j \quad \cdots \quad \hat{\mathbf{K}}_{m_s}] \mathbf{u} \quad (6)$$

where

$$\hat{\mathbf{K}}_j = \begin{cases} -\sum_{k=1}^{m_r} \left\{ \hat{f}(\varphi) \Big|_{\varphi=\varphi_{jk}} \frac{\mathbf{s}_j \times \mathbf{r}_{sk}}{|\mathbf{s}_j \times \mathbf{r}_{sk}|} \right\}, & \text{if } \mathbf{s}_j \times \mathbf{r}_{sk} \neq 0 \\ 0, & \text{if } \mathbf{s}_j \times \mathbf{r}_{sk} = 0 \end{cases} \quad (6a)$$

with $\mathbf{r}_{sk} = [\mathbf{L}_{sr}] \mathbf{r}_k$ from (4) and $\hat{f}(\varphi)$ curve fitting the torque between a PM pole pair and an EM pole pair in terms of the separation angle φ

$$\varphi_{jk} = \cos^{-1}(\mathbf{s}_j \bullet \mathbf{r}_{sk}) / (|\mathbf{s}_j| |\mathbf{r}_{sk}|). \quad (7)$$

B. Equation of Motion

The dynamic equations of motion can be derived using the Lagrangian formulation in terms of the Euler angles (α, β, γ) which have the following form:

$$[\mathbf{M}] \dot{q}_2 + \mathbf{C}(q_1, q_2) + \mathbf{C}_f = \mathbf{Q} + \mathbf{T}_{\text{ext}} \quad (8)$$

where

$$\mathbf{M} = \begin{bmatrix} I_t C_\beta^2 + I_a S_\beta^2 & 0 & -I_t S_\beta \\ 0 & I_t & 0 \\ -I_t S_\beta & 0 & I_a \end{bmatrix} \quad (8a)$$

$$\mathbf{C}(\dot{q}, q) = \begin{bmatrix} 2(I_a - I_t) S_\beta C_\beta \dot{\alpha} \dot{\beta} - I_a C_\beta \dot{\beta} \dot{\gamma} \\ (I_t - I_a) S_\beta C_\beta \dot{\alpha}^2 + I_a C_\beta \dot{\alpha} \dot{\gamma} \\ -I_a C_\beta \dot{\alpha} \dot{\beta} \end{bmatrix} \quad (8b)$$

$$\mathbf{Q} = \begin{bmatrix} -S_\beta C_\gamma & S_\beta S_\gamma & C_\beta \\ S_\gamma & C_\gamma & 0 \\ 0 & 0 & 1 \end{bmatrix} \begin{Bmatrix} T_X \\ T_Y \\ T_Z \end{Bmatrix} \quad (8c)$$

where $q_1 = [\alpha \quad \beta \quad \gamma]^T$, $q_2 = \dot{q}_1$, and \mathbf{T}_{ext} and \mathbf{C}_f are the torques imposed by external load (or disturbance) and mechanical bearing frictions, respectively. In (8a) and (8b), $I_a = I_{zz}$ and $I_t = I_{xx} = I_{yy}$ due to the symmetry, and the rotor center of gravity is assumed to coincide with the rotation center. In (8c), \mathbf{Q} represents the applied (magnetic) torque to the generalized moments in the rotor coordinates. Since the inertia matrix $[\mathbf{M}]$ is positive definite in the inclination range, $-20^\circ \leq (\alpha, \beta) \leq$

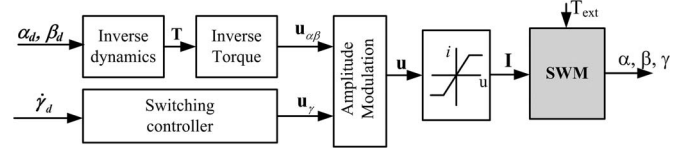


Fig. 3. OL controller of an SWM.

20° , the nonlinear dynamics (8) can be expressed in the standard state-space form

$$\dot{q} = \begin{bmatrix} \dot{q}_1 \\ \dot{q}_2 \end{bmatrix} = \begin{bmatrix} 0_{3 \times 3} & I_{3 \times 3} \\ f(q_1, q_2) & \end{bmatrix} + \begin{bmatrix} 0_{3 \times 3} \\ I_{3 \times 3} \end{bmatrix} \mathbf{Q} \quad (9)$$

where $f(q_1, q_2) = [\mathbf{M}]^{-1} \mathbf{C}(q) \in \mathbb{R}^{3 \times 1}$ is given by

$$f(q) = \frac{1}{I_t} \begin{bmatrix} \dot{\beta} \sec \beta (I_a \dot{\gamma} + (2I_t - 3I_a) \dot{\alpha} S_\beta) \\ \dot{\alpha} C_\beta (-I_a \dot{\gamma} + (I_t - I_a) \dot{\alpha} S_\beta) \\ \dot{\beta} \{-I_t \dot{\alpha} C_\beta + [I_a \dot{\gamma} + (2I_t - 3I_a) \dot{\alpha} S_\beta] \tan \beta\} \end{bmatrix}. \quad (9a)$$

III. OL CONTROLLER DESIGN

The OL SWM controller that orientates a continuously spinning rotor is shown in Fig. 3, which consists of two parts, namely, model-based inclination (α, β) control and switching spin rate $(\dot{\gamma})$ control. The amplitude-modulated current inputs to combine two parts have the form

$$u_{sj} = \text{sat}[u_{\gamma j}(1 + u_{\alpha\beta j})], \quad j = 1, 2, \dots, m_s \quad (10)$$

where $u_{\gamma j}$ governs the spin rate, $u_{\alpha\beta j}$ is an incremental factor regulating the rotor inclination about the X - and Y -axes, and $\text{sat}[\bullet]$ indicates saturation to protect the EMs.

A. Switching (Spin Motion) Controller

Two parameters are defined to facilitate the design.

- 1) Angle of plane symmetry $\psi_{\text{sym}} = \text{LCM}(\delta_r, \delta_s) \leq 180^\circ$, where LCM is the least common multiplier of its arguments: Since the EM pairs can be grouped into

$$n_{\text{sym}} = \text{int}(360^\circ / \psi_{\text{sym}}) \text{ symmetrical phases}$$

only m_s/n_{sym} input currents need to be calculated. At each switching step, n_{sym} PM pairs align with EM pairs when projected on the XY plane.

- 2) Minimum angular step $\psi_{\text{min}} = \text{GCD}(\delta_r, \delta_s)$, where GCD is the greatest common divisor of its arguments: Different step size ψ can be designed to achieve n_{max} speed levels of electronic ‘‘gear’’ transmission

$$\psi = n\psi_{\text{min}}, \quad n = 1, 2, \dots, n_{\text{max}}; \quad n_{\text{max}} = \text{int}(\delta_r / \psi_{\text{min}}).$$

For the pole pairs defined by (1) and (2), the switching sequences for $\psi = \psi_{\text{min}}$ have the form given in Table I, where all the rows repeat after every sequence number $S_N = 2m_s/n_{\text{sym}}$. By deduction, other different switching sequences for $\psi = n\psi_{\text{min}}$ can be derived from S_N as follows:

$$\text{If } S_N \leq m_s, \quad S_N = nj - (n-1), \quad j = 1, \dots, m_s$$

$$\text{If } S_N > m_s, \quad S_N = S_N - m_s.$$

TABLE I
MINIMUM-STEP SWITCHING

S_N	EM-pairs				
	1	2	3	...	m_s/n_{sym}
1	N	S	N	⋮	N
2	N	S	N		S
⋮	N	S	N		S
$m_s/n_{sym}-1$	N	S	S		S
m_s/n_{sym}	N	N	S		S
$m_s/n_{sym}+1$	S	N	S		S
$m_s/n_{sym}+2$	S	N	S		N
⋮	S	N	S		N
$2m_s/n_{sym}-1$	S	N	N		N
$2m_s/n_{sym}$	S	S	N		N

In Table I, the S_N row specifies the EM polarities. The input regulating the spin is a square wave with frequency ω_s

$$u_{\gamma j} = (-1)^j |u_{mj}| \text{sgn} [\sin(\omega_s t + \theta_j)] \quad (11)$$

where

$$\text{sgn}(x) = \begin{cases} 1, & x \geq 0 \\ -1, & x < 0 \end{cases} \quad (11a)$$

$$\omega_s = n\pi / (n_{\max} \Delta t_s) \quad (11b)$$

$$\theta_j = -\pi(n-1)/n_{\max} - jn\psi_{\min} - \theta_o. \quad (11c)$$

In (11b), Δt_s is the update sampling rate, and in (11c), $0 < \theta_o < \psi_{\min}$. The steady-state spin rate $\dot{\gamma}_{ss}$ is linearly proportional to ω_s and ψ , while the current magnitude $|u_{mj}|$ depends on the rotor dynamics.

B. Inclination Controller

As shown in Fig. 1, the SWM is structurally symmetrical, which greatly simplifies the design of an OL controller operated on a push–pull principle to maintain the rotor at an equilibrium position without any sensor feedback. The inclination (from the Z -axis) is regulated by two opposing torques such that any perturbation will result in a differential torque $\Delta \mathbf{T}$ driving the rotor to its equilibrium (like the restoring force of a spring). As will be discussed, the OL control law can be expressed in a closed form.

Push–Pull Operation: The concept of the push–pull operation, along with a general design of a spherical motor, is proposed in [21]. For this push–pull operation, the torque model is expressed in the following form:

$$\mathbf{T}_i = \mathbf{T}_{i+} + \mathbf{T}_{i-} + \Delta \mathbf{T}_i \quad (12)$$

where the subscript “ i ” denotes the torque component in the X -, Y -, or Z -direction. $\mathbf{T}_{i\pm}$ ’s are the static torques often called the “holding torque,” and $\Delta \mathbf{T}_i$ represents the “driving torque” that moves the rotor. To maintain the rotor at a particular inclination (α, β) , a “holding torque” $\mathbf{T}_{i\pm} \neq 0$ must be applied.

The principles for regulating the inclination can be summarized as follows.

- 1) To regulate the rotor at a desired steady-state orientation, the torque must satisfy the following:

$$\mathbf{T} + \mathbf{T}_L = 0, \quad \Delta \mathbf{T} = 0; \quad \|\mathbf{T}_+\| = -\|\mathbf{T}_-\| \neq 0 \quad (13)$$

where \mathbf{T}_L accounts for an external load. A change in rotor position from any equilibrium requires a differential current to be applied to generate the required $\Delta \mathbf{T}$.

- 2) To spin the rotor about its axis at a constant rate while regulating it at a desired inclination, a driving torque $\Delta \mathbf{T}_z$ must be maintained in addition to the application of the extraneous torque $\mathbf{T}_{i\pm}$.
- 3) Based on the characteristics of rotor dynamics, the rotor tends to be at the local minimum field energy states. These are local stable equilibrium positions to which the rotor would move from any perturbed position within the local boundary through the shortest path during the transient.

Solution to Redundant Inputs: The above are principles upon which the inclination controller is designed about the local equilibrium ($\alpha = \beta = \gamma = 0^\circ$). The torque required to maintain the orientation at $[\alpha = \alpha_d, \beta = \beta_d, \gamma = 0]$ is given by (5), which yields

$$\left[\tilde{\mathbf{T}}(\alpha, \beta) \right] \mathbf{u}_{\alpha\beta} = \Delta \mathbf{T}_d. \quad (13a)$$

Thus, the current vector to generate this torque is given by the inverse model

$$\mathbf{u}_{\alpha\beta} = [\tilde{\mathbf{T}}]^T \left([\tilde{\mathbf{T}}][\tilde{\mathbf{T}}]^T \right)^{-1} \Delta \mathbf{T}_d. \quad (13b)$$

Once the inclination and spin currents are computed from (11) and (13b), respectively, the total current inputs can be determined from (10).

Closed-Form OL Control Law: The Euler angles (α, β, γ) defined in Fig. 2 have intricacy in the OL controller. For the ease of visualization and deriving a closed-form OL control law, the inclination of a continuously spinning rotor is computed in real time in terms of ZYZ Euler angles $(\bar{\alpha}, \bar{\beta}, \gamma)$, where

$$\bar{\alpha} = \sin^{-1}(-S_\alpha/S_\beta) \quad \bar{\beta} = \cot^{-1}(-S_\beta C_\alpha/S_\alpha). \quad (14)$$

In this representation, $\bar{\alpha}$ is the angle of inclination between the rotor shaft and the Z -axis, $\bar{\beta}$ is the rotation of the rotor shaft (or z -axis) about the Z -axis, and γ is the spin of the rotor shaft about its own z -axis. The inclination controller is designed as follows.

- 1) The magnitude of the spin current in (11) is normalized to unity or $|u_{mj}| = 1$, which spins the rotor at $\alpha = \beta = 0$.
- 2) The required current vector to incline the rotor at other angle is given by (13b).
- 3) Two Fourier series functions (f_{j1} and f_{j2}) are defined so that the currents manipulating the $\bar{\alpha}$ and $\bar{\beta}$ motions in (10) are decoupled

$$\hat{u}_{\alpha\beta,j} = f_{j1}(\bar{\alpha})f_{j2}(\bar{\beta}) \quad (15)$$

where

$$f_{j1}(\bar{\alpha}) = \sum_{m=1}^M [a_{jm} \cos(m\bar{\alpha}) + b_{jm} \sin(m\bar{\alpha})], \quad M > 1 \quad (15a)$$

$$f_{j2}(\bar{\beta}) = c_{jo} + \sum_{m=1}^N [d_{jm} \cos(m\bar{\beta}) + e_{jm} \sin(m\bar{\beta})], \quad N > 1. \quad (15b)$$

The coefficients of the Fourier series in (15a) and (15b) are found by minimizing the following square-error function:

$$E_j = (u_{\alpha\beta,j} - \hat{u}_{\alpha\beta,j})^2. \quad (16)$$

Since the *ZYZ* Euler angle representation has a singularity at $\bar{\alpha} = \bar{\beta} = 0$ (namely, the angles $\bar{\alpha}$ and γ are coincident at $\bar{\beta} = 0$, and thus, the controller cannot distinguish between two angles), it is used only to obtain (15) in a closed form for the inclination control at $\beta \neq 0$.

The OL inclination controller (15) is designed by minimizing (16) for the computation domain, where the indices M and N in (15) are determined by limiting the maximum error (16) to a specified criterion. The two parameters ($\bar{\alpha}$ and $\bar{\beta}$) are optimized using the linear least square method in the MATLAB optimization. However, (15) and (16) are insufficient to determine a unique solution, and also, the computation is time consuming. For an SWM, $\bar{\alpha}$ typically has a finite range within which $u_{\alpha\beta,j}$ is proportional to $\bar{\alpha}$. Based on this observation, the optimization employs the following steps.

- 1) Set $f_{j1}(\bar{\alpha}) = 1$ at a specified $\bar{\alpha} = \bar{\alpha}_o$ within the range.
- 2) By using a least square fit, find $f_{j2}(\bar{\beta})$ to fit u at $\bar{\alpha} = \bar{\alpha}_o$.
- 3) Update $f_{j1}(\bar{\alpha})$ with the result of $f_{j2}(\bar{\beta})$ in step 2).
- 4) Repeat step 2) using $f_{j1}(\bar{\alpha})$ from step 3) until (16) is less than a specified error criterion.

C. Design Example

To illustrate the procedure of designing the OL controller (Fig. 3), the SWM (Fig. 1) has been utilized with two layers of eight PMs on the rotor and two layers of ten EMs on the stator. Other parameters that characterize the electrical and mechanical components are detailed in Table II. The ten EM pairs are divided into two symmetrical phases, implying that the sixth to tenth EMs have the same current profiles as the first to fifth EMs, respectively. In addition, five different spin-speed levels can be defined in terms of $\psi = n\psi_{\min}$ as discussed in Section III-A, where $n = 1, 2, \dots, n_{\max}$, $n_{\max} = 5$, and $\psi_{\min} = 9^\circ$.

Table III illustrates the EM layout plan view and lists the switching sequences of the five speed levels, which are intuitively derived as follows.

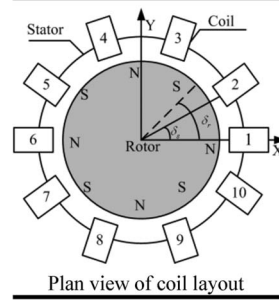
- 1) From Table I, obtain the current polarity for the timing diagram of the switching current vector \mathbf{u}_γ in Fig. 4, where the horizontal axis indicates S_N (that is also the time step).
- 2) For a particular speed level n , the switching period T , which depends on the number of sequences S_N , is given in terms of sampling interval Δt_s in Table III.

TABLE II
STATOR AND ROTOR POLE PAIRS OF THE SWM (FIG. 1)

Rotor	2 layers of 8 PMs
radius	76.2 mm (3 inches)
Cylindrical PM	OD=L=12.5mm (0.5in)
Magnetization	$\phi_r = 20^\circ$; $\delta_r = 45^\circ$; $\mu_0 M_0 = 1.35$ Tesla
Stator	2 layers of 10 EMs
Cylindrical EM	OD = 18.8mm (0.75 in), 1050 turns, 6.46Ohms
Magnetization	$\phi_s = 26^\circ$; $\delta_s = 36^\circ$; AWG 29 Coil wire
Current	0.5 A through 2 EMs in series; $u_{sat} = 1$ Amp
Air-gap between EM & PM:	0.762mm (0.03in)
Moment of rotor inertia (kg-m ²):	$I_a = 6.0576e-005$; $I_r = 3.8628e-005$
Frictional coefficient C_f :	0.3 Nm•sec
Offset of mass centre: $\bar{r} = 0$	
$\psi_{sym} = 180^\circ \Rightarrow n_{sym} = 2$ phases	
$\psi_{\min} = 9^\circ \Rightarrow n_{\max} = 5 (= 45/9)$ spin-speed levels	

TABLE III
SWITCHING CONTROLLER FOR $n = 1, 2, \dots, 5$ SPIN-SPEED LEVELS

n	ψ	S_N	Period, T
1	9°	1, 2, 3, 4, 5, 6, 7, 8, 9, 10	$90^\circ, 10\Delta t_s$
2	18°	1, 3, 5, 7, 9	$90^\circ, 5\Delta t_s$
3	27°	1, 4, 7, 10, 3, 6, 9, 2, 5, 8	$270^\circ, 10\Delta t_s$
4	36°	1, 5, 9, 3, 7	$180^\circ, 5\Delta t_s$
5	45°	1, 6	$90^\circ, 2\Delta t_s$



- 3) For each time step, the rotor spins $\psi = n\psi_{\min}$ degrees, and the rotor requires $360/\psi$ steps to complete one revolution. Thus, the spin rate (in revolutions per minute) directly depends on n and Δt_s . Table IV shows the examples of the spin rates in relation to the parameters in (11) for $\theta_o = 5^\circ$ and $\Delta t_s = 1$ ms.

The switching current can also be expressed mathematically by (11), where ω_s and θ_j are given in Table IV.

As outlined in Section III-B, the two controller parameters for range of motion ($0 \leq \bar{\alpha} \leq 6^\circ$ and $0 \leq \bar{\beta} \leq 360^\circ$) are optimized using the linear least square method of the MATLAB optimization toolbox with $\Delta\bar{\alpha} = 1^\circ$ and $\Delta\bar{\beta} = 3^\circ$. The indices were determined to be $M = 2$ and $N = 3$ for a maximum error of less than 5%. In step 1) of the optimization procedure, $\bar{\alpha} = \bar{\alpha}_o = 5^\circ$ was initially chosen because $u_{\alpha\beta,j}$ is proportional to $\bar{\alpha}$ for its small range but fluctuates largely with $\bar{\beta}$. In addition, once a pair of PM and EM is aligned at $\bar{\alpha} = \phi_s - \phi_r = 6^\circ$, the aligned pole pair generates no tangent force, and thus, the inclination current cannot be determined. The computed ($\bar{\alpha}$ and $\bar{\beta}$) values at no load are detailed in Table V. The computed current profiles flowing through the first to fifth EMs for regulating the inclination in OL are shown in Fig. 5.

Due to the symmetrical structure designed to operate on the push-pull principle, it can be shown using (13b) that the currents in the sixth to tenth EMs have equal magnitude but opposite direction as those to the first to fifth EMs. Similar arguments can be made for the pairs $j = 2, 5$ and $j = 3, 4$ which are mirror images as shown in Fig. 7.

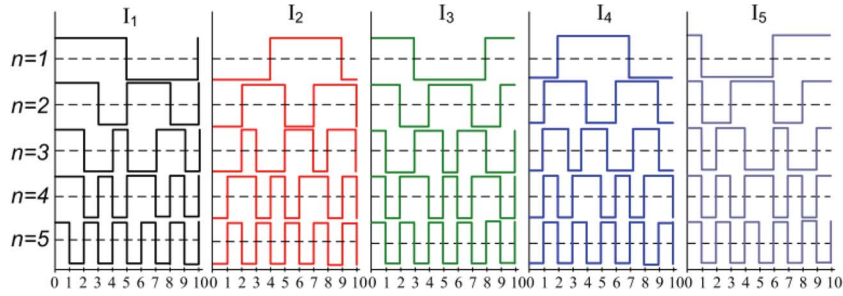


Fig. 4. Timing diagram for five different spin-speed levels.

TABLE IV
PARAMETERS OF SWITCHING CONTROLLER
(AT $\theta_o = 5^\circ$ AND $\Delta t_s = 1$ ms)

n	θ_j (rad)	ω_s (rad/s)	T (ms)	$\dot{\gamma}_{ss}$ rpm
1	$-0.1571j-0.0873^*$	628	10	1500
2	$-0.3142j-0.7156$	1,257	5	3000
3	$-0.4713j-1.3439$	1,885	10	4500
4	$-0.6284j-1.9723$	2,513	5	6000
5	$-0.7855j-2.6006$	3,142	2	7500

* j denotes the j^{th} EM pair in the stator defined in (2).

TABLE V
FOURIER SERIES CONSTANT FOR THE INCLINATION

$\bar{\alpha}$ current vector					
j	1	2	3		
a_{i1}	6374.87	5162.52	3843.15		
a_{i2}	-3185.02	-2579.32	-1919.34		
b_{i1}	-134.896	-144.083	-101.69		
b_{i2}	134.89	144.074	101.682		
$\bar{\beta}$ current vector					
j	1	2	3	4	5
c_{i0}	0.035466	-0.091224	-0.003365	-0.003365	-0.091224
d_{i1}	0.02134	-0.130895	0.013119	-0.036560	-0.12672
d_{i2}	-0.09967	0.040402	0.005075	-0.003483	0.055141
d_{i3}	-0.01214	-0.054836	0.003483	-0.005075	-0.048777
e_{i1}	-0.47508	0.126491	0.03656	0.013119	-0.142679
e_{i2}	-0.02024	0.165207	-0.032600	0.032600	-0.158953
e_{i3}	0.118731	0.032188	-0.023501	0.023501	-0.037096

due to the symmetry about $\bar{\alpha}$, $u_{\alpha\beta,5} = u_{\alpha\beta,2}$, $u_{\alpha\beta,4} = u_{\alpha\beta,3}$

IV. EXPERIMENTAL RESULTS

To validate the control law (10) and forward/inverse torque models [see (6) and (13b)], for the OL-controlled SWM, the OL controller (Fig. 3) is evaluated by experimentally determining the dynamics of the prototype SWM shown in Fig. 6, where the design parameters are numerically defined in Table II.

The control systems are implemented on a personal computer completed with two 8-channel D/A and 16-channel A/D conversion boards as described in Table VI. The rotor inclination is measured by four linear single-axis Hall-effect UGN3505 sensors. The signals from the Hall-effect sensors (proportional to the measured magnetic field) are amplified before digitized by the PCI-DAS6036, which are bipolar ranging from ± 500 mV to ± 10 V and thus capable of measuring both the north and south polarities of the magnetic field. Details of the orientation measurement can be found in [20].

The updating and settling times for the transient responses in each channel are 10 and 15 ms, respectively. These update speeds limit the maximum spin rate as well as the square-wave

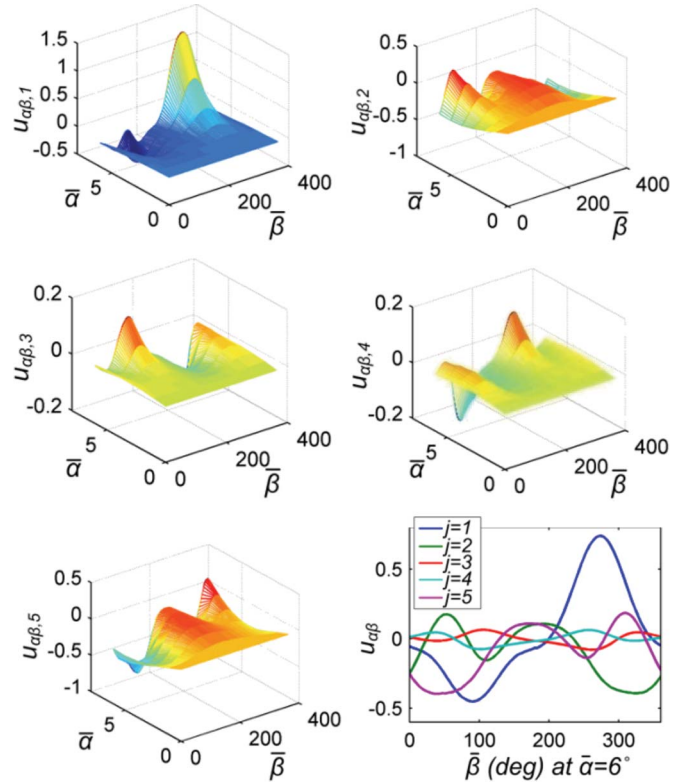


Fig. 5. Current inputs for inclination controller.



Fig. 6. SWM. (a) Rotor. (b) Stator.

TABLE VI
SYSTEM PARAMETERS

System I/O	# channels	Range	Update time	Data Bit
KPCI-3130	8 D/A	-3.5- 3.5A	15ms	8-bit (reg)
PCI-DAS6036	16 A/D	-10 - 10V	5μs	16 bit
Measurement	# axis	V _{cc} *	V _{out} *	Sensitivity
UGN3505	1	5V	0.2 - 4.7V	2.5mV/G

* V_{cc} is the supply voltage; V_{out} is the output voltage range

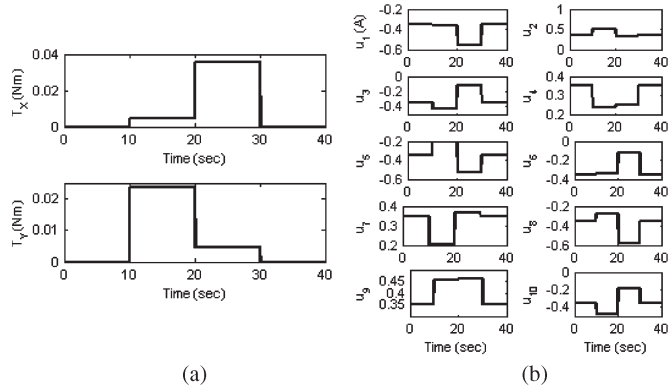


Fig. 7. OL control using step input. (a) Inclination torques. (b) Applied current inputs.

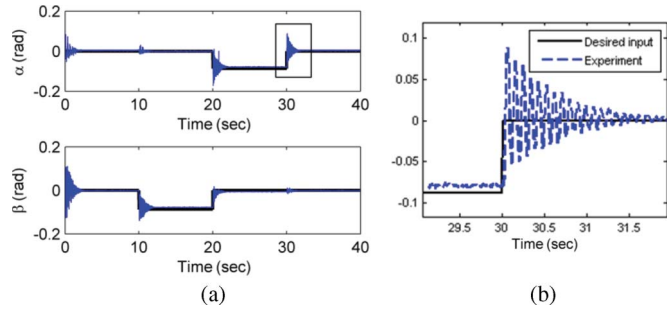


Fig. 8. Step response of the OL control. (a) Step response in OL control. (b) Transient response.

TABLE VII
TRANSIENT RESPONSES

	t_r (sec)	M_p (%)	t_s (sec)	e_{ss} (rad)
OL	0.04	95	1.67	0.007

frequency for the switching control (11). Without loss of generality, the current input is limited to 1 A to avoid incidentally overheating the EM coils. With this in mind, the following tasks in Sections IV-A and B were tested.

A. Inclination Control Only

The rotor was initialized from an arbitrary state to the equilibrium operating state ($\alpha = \beta = \gamma = 0^\circ$; Z - and z -axes coincide, and EM pair #1 and #6 is aligned with a PM pair as shown in Table III) by energized coils ($j = 1, 3, 4, 6, 8, 9$ in Table III) with the same polarities. Once initialized, it was commanded to ($\alpha = 5^\circ, \beta = 0$) and then to its final inclination ($\alpha = 5^\circ, \beta = 5^\circ$).

Each command is a 5° step input for apparent comparison. To accomplish this task, the torque required to incline the rotor is solved from the inverse dynamics in (8), upon which the current input vector $\mathbf{u}_{\alpha\beta}$ is calculated from (13) and (15). Fig. 7 shows the computed torques and the applied current inputs. The step response results of $\alpha(t)$ and $\beta(t)$ are shown in Fig. 8 and Table VII, where t_r , t_s , M_p , and e_{ss} are the rise time, 2% settling time, percentage overshoot, and steady-state error, respectively. Clearly, the square wave resembles a repetitive step input that provides a basis to evaluate the SWM dynamic performance. A portion of the step responses

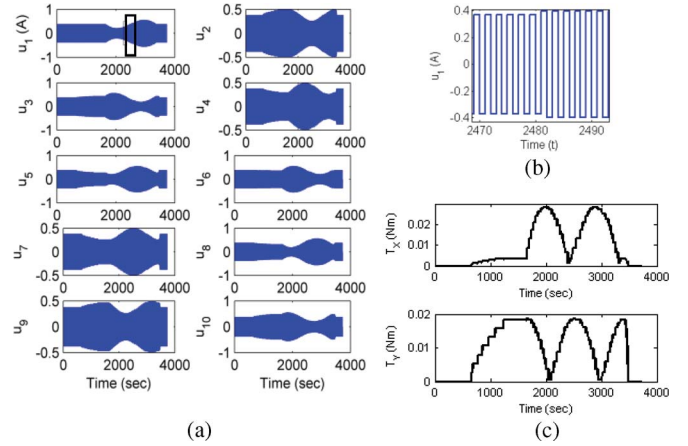


Fig. 9. Current inputs and torque. (a) Current inputs. (b) Zoom-in view of (a). (c) Inclination torques.

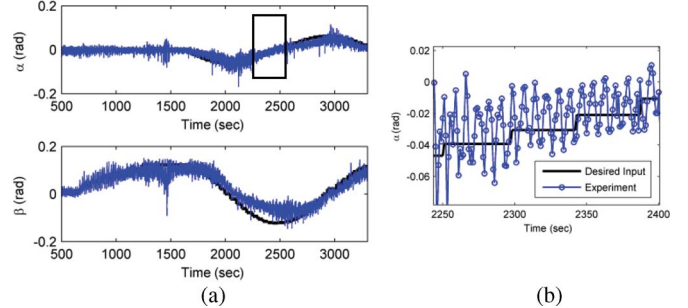


Fig. 10. Orientation of the continuously spinning shaft. (a) Tacking outputs. (b) Zoom-in view of (a).

is enlarged in Fig. 8(b) for transient response analyses, where both the initial and final inputs are predestined. As expected, the spherical motor exhibits significant overshoot because of its low mechanical damping characteristics. Overshoot can be damped out electronically (using inputs with smooth waveforms) or by means of software through techniques such as input shaping.

B. Spin at a Specified Inclination

This is similar to experiment A except that the rotor spins at 300 r/min while inclining along a specified trajectory. Since the spin is controlled in OL, the effect of gyroscopic moment on the spin must be minimized to maintain the rotor stability. For this reason, the following trajectory is used for this test.

- 1) The 45° spin controller for the highest speed level ($n_{\max} = 5$) is applied to spin the rotor at 185 r/min and then gradually increase to 300 r/min while maintaining the inclination at ($\alpha = 5^\circ, \beta = 0^\circ$).
- 2) The rotor is then commanded to move along a desired circular trajectory while spinning at 300 r/min.

Fig. 9(a) and (b) shows the input currents calculated from (10), (13b), and (15) for the required torques in Fig. 9(c). The experimental responses are shown in Fig. 10.

C. Discussion of Results

Some observations can be made from Figs. 8–10.

- 1) As the magnetic field/torque (and, hence, $\mathbf{u}_{\alpha\beta}$) to maintain the desired inclination can be effectively predicted

from the DMP method (and the inverse dynamics), the OL controller offers an accurate steady-state inclination (with no spin motion) as shown in Fig. 8.

- 2) Unlike $\mathbf{u}_{\alpha\beta}$, the \mathbf{u}_γ computation is based on kinematics. The unmodeled dynamics and input current approximations [see (15a) and (15b)] result in some slow drifts in the inclination.
- 3) Persistent oscillations (with a period proportional to the spinning speed) can be observed in Fig. 10, implying that the square-wave switching input generates torque ripple and has an effect on the spin motion.

The system has some mechanical imperfections. Most notably are the uneven coil windings that contribute to nonuniform air gap between the rotor and the stator. This, along with static friction uncertainties in the bearing, accounts for the nonconcentric motion in Fig. 10.

V. CONCLUSION

This paper has presented a method to design an OL controller of an SWM that is capable of controlling its orientation of a continuously rotating shaft. In particular, the OL control presented here offers an effective means to decouple the control of the spin motion from that of the inclination and thus allow the OL controller to consist of two independent parts, namely, a switching (spin-rate) controller based on the principle of a stepper for maintaining the spin rate and an inclination controller based on the inverse torque model and the push-pull principle for regulating the rotor inclination. The feasibility of the OL-controlled SWM has been experimentally demonstrated with 16 rotor PMs and 20 EMs of the SWM. The experimental results not only prove the OL controller of the SWM but also provide intuitive insights into the effects of key operation parameters on the SWM dynamics. Thus, the results presented here will serve as a basis for developing feedback controllers to achieve accurate positioning and disturbance rejection.

REFERENCES

- [1] F. Baronti, F. Lenzi, R. Roncella, R. Saletti, and O. Di Tanna, "Electronic control of a motorcycle suspension for preload self-adjustment," *IEEE Trans. Ind. Electron.*, vol. 55, no. 7, pp. 2832–2837, Jul. 2008.
- [2] C. Gerada and K. J. Bradley, "Integrated PM machine design for an aircraft EMA," *IEEE Trans. Ind. Electron.*, vol. 55, no. 9, pp. 3300–3306, Sep. 2008.
- [3] K.-M. Lee and C. Kwan, "Design concept development of a spherical stepper for robotic applications," *IEEE Trans. Robot. Autom.*, vol. 7, no. 1, pp. 175–181, Feb. 1991.
- [4] R. L. Hollis, S. E. Salcudean, and A. P. Allan, "A six degrees-of-freedom magnetically levitated variable compliance fine-motion wrist: Design, modeling, and control," *IEEE Trans. Robot. Autom.*, vol. 7, no. 3, pp. 320–332, Jun. 1991.
- [5] N. Hoshi and A. Kawamura, "Analysis of primary-on-slider type piezoelectric actuator and the application to two degree-of-motion freedom plane actuator," *IEEE Trans. Ind. Electron.*, vol. 43, no. 1, pp. 192–196, Feb. 1996.
- [6] K. Kahlen, I. Voss, C. Priebe, and R. W. D. Doncker, "Torque control of a spherical machine with variable pole pitch," *IEEE Trans. Power Electron.*, vol. 19, no. 6, pp. 1628–1634, Nov. 2004.
- [7] K.-M. Lee, H. Son, and J. Joni, "Concept development and design of a spherical wheel motor (SWM)," in *Proc. IEEE ICRA*, Barcelona, Spain, 2005, pp. 18–22.
- [8] M. K. Rashid and Z. A. Khalil, "Configuration design and intelligent stepping of a spherical motor in robotic joint," *J. Intell. Robot. Syst.*, vol. 40, no. 2, pp. 165–181, Jun. 2004.
- [9] K.-M. Lee, R. A. Sosseh, and Z. Wei, "Effects of the torque model on the control of a VR spherical motor," *IFAC J. Control Eng. Pract.*, vol. 12, no. 11, pp. 1437–1449, Nov. 2004.
- [10] C. K. Lim, I.-M. Chen, L. Yan, G. Yang, and K.-M. Lee, "Electromechanical modeling of a permanent-magnet spherical actuator based on magnetic-dipole-moment principle," *IEEE Trans. Ind. Electron.*, vol. 56, no. 5, pp. 1640–1648, May 2009.
- [11] C. Xia, P. Song, H. Li, B. Li, and T. Shi, "Research on torque calculation method of permanent-magnet spherical motor based on the finite-element method," *IEEE Trans. Ind. Electron.*, vol. 45, no. 4, pp. 2015–2022, Apr. 2009.
- [12] L. Yan, I. M. Chen, C. K. Lim, G. Yang, L. Wei, and K.-M. Lee, "Design and analysis of a permanent magnet spherical actuator," *IEEE/ASME Trans. Mechatronics*, vol. 13, no. 2, pp. 1437–1449, Apr. 2008.
- [13] C. Xia, H. Li, and T. Shi, "3-D magnetic field and torque analysis of a novel Halbach array permanent-magnet spherical motor," *IEEE Trans. Magn.*, vol. 44, no. 8, pp. 2016–2019, Aug. 2008.
- [14] B. Ackermann, H. Steinbusch, T. Vollmer, J. Wang, G. W. Jewell, and D. Howe, "A spherical permanent magnet actuator for a high-fidelity force-feedback joystick," *IEEE/ASME Trans. Mechatron.*, vol. 14, no. 3, pp. 327–339, Apr. 2004.
- [15] M.-Y. Chen, M.-J. Wang, and L.-C. Fu, "Modeling and controller design of a maglev guiding system for application in precision positioning," *IEEE Trans. Ind. Electron.*, vol. 50, no. 3, pp. 493–506, Jun. 2003.
- [16] A. Forrai, T. Ueda, and T. Yumura, "Electromagnetic actuator control: A linear parameter-varying (LPV) approach," *IEEE Trans. Ind. Electron.*, vol. 54, no. 3, pp. 1430–1441, Jun. 2007.
- [17] T. Miura and T. Taniguchi, "Open-loop control of a stepping motor using oscillation-suppressive exciting sequence tuned by genetic algorithm," *IEEE Trans. Ind. Electron.*, vol. 46, no. 6, pp. 1192–1198, Dec. 1999.
- [18] Y. A.-R. I. Mohamed, "A newly designed instantaneous-torque control of direct-drive PMSM servo actuator with improved torque estimation and control characteristics," *IEEE Trans. Ind. Electron.*, vol. 54, no. 5, pp. 2864–2873, Oct. 2007.
- [19] K.-M. Lee and H. Son, "Distributed multi-pole model for design of permanent-magnet based actuators," *IEEE Trans. Magn.*, vol. 43, no. 10, pp. 3904–3913, Oct. 2007.
- [20] H. Son and K.-M. Lee, "Distributed multi-pole model for real-time control and motion simulation of PM-based actuators," *IEEE/ASME Trans. Mechatron.*, vol. 13, no. 2, pp. 228–238, Apr. 2008.
- [21] K.-M. Lee and H. Son, "Torque model for design and control of a spherical wheel motor," in *Proc. IEEE/ASME Int. Conf. Adv. Intell. Mechatronics*, 2005, vol. 1, pp. 335–340.



Hungsun Son (S'07–M'09) received the M.S. degree in aeronautical and astronautical engineering from Stanford University, Stanford, CA, in 2002 and the Ph.D. degree in mechanical engineering from the Georgia Institute of Technology, Atlanta, in 2008.

He is currently an Assistant Professor in aerospace and mechanical engineering with Nanyang Technological University, Singapore. His current research interests include mechatronics, sensors and actuators, dynamic system modeling, design optimization, automation, and control.



Kok-Meng Lee (M'89–SM'02–F'05) received the B.S. degree from the State University of New York, Buffalo, in 1980 and the M.S. and Ph.D. degrees from the Massachusetts Institute of Technology, Cambridge, in 1982 and 1985, respectively.

He is currently a Professor with the George W. Woodruff School of Mechanical Engineering, Georgia Institute of Technology, Atlanta. He is the holder of eight patents in machine vision, 3-DOF spherical motor/encoder, and live-bird handling system. His research interests include system dynamics/control, robotics, automation, and mechatronics.

Dr. Lee is a Fellow of the American Society of Mechanical Engineers. He received the National Science Foundation Presidential Young Investigator, Sigma Xi Junior Faculty Research, International Hall of Fame New Technology, and Kayamori Best Paper Awards.